Article

Journal of
Nanoscience and Nanotechnology
Vol. 17, 1547–1554, 2017
www.aspbs.com/jnn



# Dispersion of Multi-Walled Carbon Nanotubes in Skutterudites and Its Effect on Thermoelectric and Mechanical Properties

Andreas Schmitz[1,*], Carolin Schmid[1], Johannes de Boor[1], and Eckhard Müller[1,2]

[1] *Institute of Materials Research, German Aerospace Center, Linder Hoehe, 51147 Koeln, Germany*
[2] *Institute for Inorganic and Analytical Chemistry, Justus-Liebig-University, Heinrich-Buff-Ring 58, 35392 Giessen, Germany*

Filled cobalt-antimony based skutterudites have proven themselves as very promising thermoelectric materials for generator applications in an intermediate temperature range between 400 and 800 K due to their high figure of merit. Besides the functional thermoelectric properties also the skutterudites' mechanical properties play an important role to withstand external mechanical and internal thermomechanical loads during operation. Properties of interest are hardness as well as fracture toughness and resistance to fatigue. Carbon nano tubes are well known for their high tensile strength and may therefore be used to increase the mechanical strength of composite materials. Additionally, the thermoelectric properties of the composite material might benefit from the high electrical conductivity of carbon nano tubes and increased phonon scattering at interfaces between matrix and carbon nano tube. A main precondition for benefiting from embedded nanotubes is to achieve a homogeneous distribution of the CNTs and good adhesion between carbon nano tube and matrix material. In this work we present the influence of the introduction of multi-walled carbon nano tubes on the thermoelectric and mechanical properties of *p*-type skutterudites $Ce_{0.14}La_{0.06}Co_2Fe_2Sb_{12}$. The influence of different carbon nano tube concentrations and preparation routes on the resulting composite material's thermoelectric, mechanical and microstructural properties is studied. A reduction of electrical and thermal conductivity as well as fracture strength is observed with increasing carbon nano tube content which is attributed to strong agglomeration of the nano tubes. The results underline the pivotal role of a homogeneous distribution of the carbon nano tubes for improving the mechanical properties of skutterudites.

**Keywords:** Thermoelectricity, Skutterudites, Carbon Nano Tubes, Thermoelectric Properties, Mechanical Properties.

## 1. INTRODUCTION

Thermoelectric energy conversion with skutterudites as one of the most promising thermoelectric materials enables the direct conversion of heat into electricity.[1–3] This technology therefore has great potential in waste energy recovery and in increasing the efficiency of many industrial processes to reduce primary energy consumption and $CO_2$ emissions.[4] The thermoelectric functional properties are described by a material's Seebeck coefficient $S$, electrical conductivity $\sigma$ and thermal conductivity $\kappa$. These can be summarized in the thermoelectric figure of merit $ZT$.[5] Of equal importance for applications using these materials are the mechanical properties such as hardness, Young's modulus or yield strength.[6]

Skutterudites are typically hard and brittle which might result in abrupt complete failure of a skutterudite based thermoelectric generator during operation.[7,8] High brittleness is typical for most thermoelectric materials. Therefore, improving the fracture behavior is a major task common for many thermoelectric materials. One approach to achieve this, is combining skutterudites with micro or nano scaled fibers or ceramic inclusions to hinder crack growth or even bridge cracks.[9] Additionally, these inclusions can also potentially be beneficial for the

*Author to whom correspondence should be addressed.

thermoelectric properties by altering the microstructure of the material, thus—for example—leading to increased phonon scattering and consequently reduced thermal conductivity.[9–14]

Wan et al. reported enhanced thermoelectric and mechanical properties of *p*-type $CeFe_4Sb_{12}$ skutterudite compounds due to short carbon nanofibers.[9] They achieved a homogeneous distribution of these fibers in the skutterudite matrix and observed a strong increase of the composite's fracture toughness. Due to their extraordinary mechanical properties and nano scale, carbon nano tubes (CNT) have the potential for composite materials with even better properties.[15, 16] Here separation and dispersion of the CNTs is a main issue due to the strong Van-der-Waals interaction between the CNTs resulting in the formation of agglomerates.[17–19]

Ren et al. report strongly increased mechanical strength and good thermoelectric properties in bismuth antimony telluride with carbon nano tubes.[20] Several publications describe increased Seebeck coefficients and reduced thermal conductivity in composites of thermoelectric materials—mainly tellurides—and carbon nano tubes.[21–24]

In this work we present two different routes to disperse multi-walled carbon nano tubes in a skutterudite matrix material and investigate the thermoelectric and mechanical properties of the resulting composites. The results show that CNTs have a good potential for increasing the thermoelectric performance even if the CNTs are not fully homogeneously dispersed in the matrix, while increased mechanical stability can only be achieved if the nano tubes are well dispersed and embedded in the matrix material.

## 2. EXPERIMENTAL DETAILS

Cerium and lanthanum were chosen as filler elements. Both have proven themselves as very promising fillers.[25–27] Furthermore, cerium and lanthanum with ratios close to 2:1 are the main constituents of the cheap and readily available so called "Mischmetall," which might be an interesting option as filler in skutterudites for mass market TE applications. Thus, for this work elements (Ce, La, Fe, Co, Sb) of purity 5 N were weighed according to the stoichiometry $Ce_{0.14}La_{0.06}Co_2Fe_2Sb_{12}$ under argon atmosphere and then sealed in evacuated quartz ampoules. The high iron content was chosen in order to achieve high hole concentrations and thus good electrical conductivity. The material was then molten in a rocking furnace for 2 hours at 1150 °C before quenching in water. Afterwards, the ingots were annealed inside the quartz ampoules for seven days at 650 °C. The material was then ground and sieved to achieve powder particles smaller than 50 $\mu$m. A *BeckmanCoulter LS13320* particle analyzer was used to determine the particle size distribution in the powder and a *Siemens Bruker D5000* powder XRD system (Cu K$\alpha$ radiation) plus *Fullprof* software was used for phase identification and refinement.[28] All composite and reference samples were prepared from the same powder batch to avoid any misleading variations and effects of composition or particle size distribution.

Commercial multi-walled carbon nano tubes *"Baytubes C70 P"* were used in this work. These nano tubes are >95 wt% pure CNTs with inner and outer diameters of 4 and 13 nm, respectively, and a length of >1 $\mu$m. Two different routes were chosen for mixing the nano tubes and skutterudite powder: first, the CNTs were ground together with the skutterudite powder by hand in an agate mortar ("pestle-only preparation"). This route involves minimal mechanical stress to the CNTs thus keeping their original length and surface. Second, CNTs were suspended in Ethanol at 60 °C. Ultrasonic treatment was used for ten minutes to break any agglomerates, while after five minutes the skutterudite powder was added to the suspension. The chosen duration of ultrasonic treatment was found to be sufficient to break agglomerates and short enough to avoid severe mechanical damage to the CNT walls.[19] The mixture was then dried at 60 °C in a furnace. Samples prepared by this route will be nominated "ultrasonic preparation."

CNT concentrations of 0.5, 1.0 and 1.5 wt% in the skutterudite matrix were prepared by each preparation route. The composite material was then sintered under vacuum at 550 °C with a current assisted short-term sintering approach using a *"Dr. Fritsch DSP-510SE"* sintering machine.[29] Samples of 12.7 mm diameter and 1.5 mm thickness were prepared for thermoelectric measurements. Furthermore, samples of 15.0 mm diameter and 4.0 mm thickness were sintered for mechanical characterization. Those samples were later cut into cubes of $4 \times 4 \times 4$ mm$^3$ for compression tests and bars of $2 \times 4 \times 15$ mm$^3$ for bending tests.

Room temperature scans of the Seebeck coefficient on the original ingot and sintered samples were performed using a Potential and Seebeck Microprobe (PSM) to check the material's homogeneity.[30] The temperature dependent thermal conductivity $\kappa$ was measured with a *Netzsch LFA 427*. Archimedes' principle was used to determine the sample density, and Dulong-Petit's law for calculating the heat capacity (0.235 J/gK). The CNT contribution to the heat capacity is neglected due to their small contribution at the investigated concentrations. The temperature dependent Seebeck coefficient $S$ and electrical conductivity $\sigma$ were measured concurrently using a custom-built measurement device.[31] To obtain information on the stability of the material's functional properties, all three properties were recorded during the heating and cooling phase of the measurement cycles. Measurement errors are assumed to be 8%, 2% and 5% for $\kappa$, $\sigma$ and $S$, respectively. The 5% error of $S$ mainly accounts for accuracy and thus a potential absolute error of the measured values due to systematic errors. Repeatability of the Seebeck coefficient measurement is better allowing the identification of smaller differences between samples.[32] Hall measurements at room

temperature were performed on a custom-built measurement device using van-der-Pauw geometry.

Vickers hardness measurements using an indentation force of 0.49 N were performed at room temperature on polished samples and averaged over 50 indentations, 25 on each side of the sintered pellets. Uniaxial compression tests were performed at room temperature on cubes of $4 \times 4 \times 4$ mm$^3$ using an *Instron 5966* machine at 0.5 mm/s and a travel sensor attached to the sample holder. Furthermore, 4-point-bending tests were performed at room temperature using the same machine.

Scanning electron microscopy plus EDX was used to investigate the microstructure on polished samples as well as fracture surfaces resulting from the mechanical tests.

## 3. RESULTS AND DISCUSSION

Before mixing with CNTs, the skutterudite powder has a broad particle size distribution with significant volumetric contributions of particles in the size range from 0.7 to 70 $\mu$m (see Fig. 1). The short grinding together with the CNTs in the pestle-only route has no significant influence on the particle size distribution.

The XRD measurements shown in Figure 2 reveal secondary $FeSb_2$ and Sb phases. No publication on the filling and solubility limits of Ce and La double-filled skutterudites are known to the authors. Therefore, a high Fe content and moderate filling was chosen to achieve high hole concentrations and thus good electrical conductivity. Based on publications on Ce or La single-filled skutterudites, the observed formation of precipitates might indicate that the chosen amount of iron might be above the solubility limit of Fe in $CoSb_3$ at the given rare earth filling.[25, 33, 34] EDX/SEM measurements indicate a composition of $Fe_{1.6}Co_{2.4}Sb_{12}$ in the skutterudite phase and secondary phases with compositions $Fe_{0.8}Co_{0.2}Sb_2$ and pure antimony in precipitates of 1 to 10 $\mu$m in size. As no lanthanum or cerium rich phases were detected, it is expected that both elements are dissolved in the skutterudite phase as filler atoms. This cannot be resolved by EDX due to the low concentration of lanthanum and cerium in the skutterudite phase.

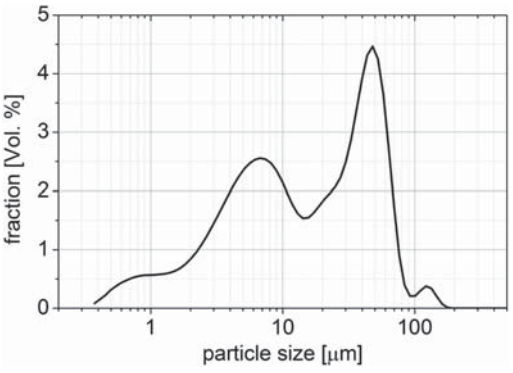


**Figure 1.** After grinding the skutterudite powder has a broad particle size distribution with particle sizes ranging from 0.7 $\mu$m to 70 $\mu$m.

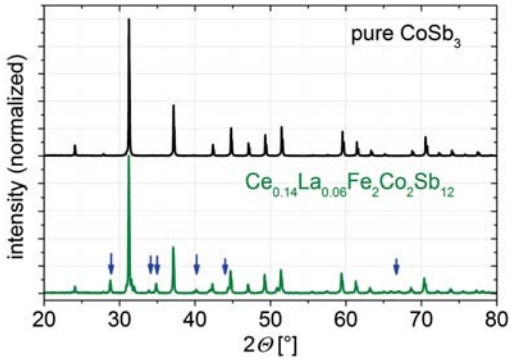


**Figure 2.** Comparison of XRD powder diffraction patterns of pure $CoSb_3$ skutterudite (top) and $Ce_{0.14}La_{0.06}Fe_2Co_2Sb_{12}$ powder used in this study (bottom). Arrows indicate peaks of secondary phases, mainly $FeSb_2$ and Sb and potentially minor amounts of $CoSb_2$.

As can be seen in Figure 3, except for one all sintered samples have relative densities above 97%. Here, the theoretical density was calculated as weighted average between skutterudite and CNT, assuming an average of 9 walls for each CNT.[35] Agglomeration of CNTs is expected to significantly reduce the density, as these agglomerates contain a loose network of CNTs with empty spaces in between, which will not be filled by the skutterudite powder during sintering. As can be seen, samples sintered from the powder subject to ultrasonic treatment tend to have slightly higher densities thus indicating better dispersion and embedding of the CNTs in the skutterudite matrix of these samples. Still, large agglomerates of CNTs in the size range up to 0.8 mm can be seen on all samples after polishing. These large agglomerates are also visible as spots with low Seebeck coefficient in room temperature surface scans of the Seebeck coefficient

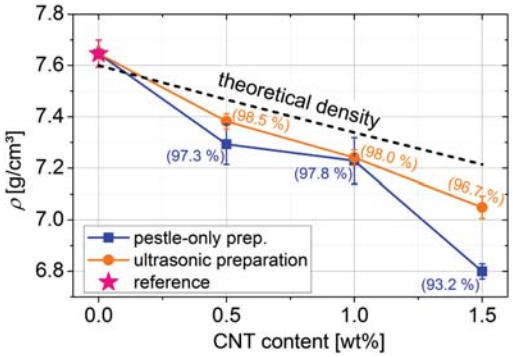


**Figure 3.** Density of all sintered samples. The dashed line indicates the theoretical density calculated for the CNT-skutterudite-composites; numbers indicate the relative density of the sintered samples based on this theoretical density. Densities exceed 97% of the theoretical density in all samples except for the sample containing 1.5 wt% CNT prepared by pestle-only preparation.

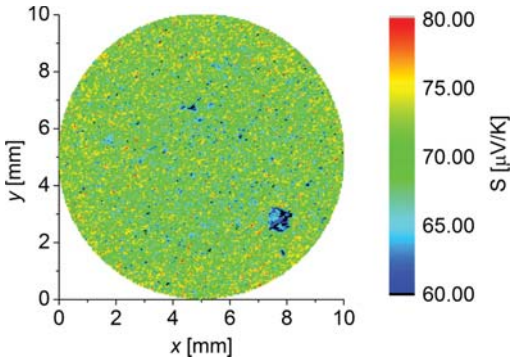


**Figure 4.** Distribution of the room temperature Seebeck coefficients on the surface of a sample containing 1.0 wt% CNT prepared by ultrasonic preparation. The sample is macroscopically homogeneous with small fluctuations on a micrometer scale. Blue areas indicate differently sized agglomerates of CNTs.

(Fig. 4). Furthermore, these scans proof that apart from these agglomerates all samples are homogeneous, as exemplary displayed in Figure 4 for the 1.0 wt% CNTs ultrasonic preparation sample.

As can be seen in Figure 5, the Seebeck coefficient is positive and increases with temperature in all samples. This behaviour is expected as iron acts as electron acceptor in $CoSb_3$ based skutterudites.[36, 37] Furthermore, all samples are stable during the measurements, as can be seen by the nearly perfect match of the data recorded during heating and cooling phases of the measurement cycles. The carbon nanotubes lead to an increase of the Seebeck coefficient, which appears independent of the CNT concentration and preparation route. This is in good agreement to similar findings by Ren et al. in thermoelectric composites of $Bi_{0.4}Sb_{1.6}Te_3$ with CNTs and by Truong et al. in $MnSi_{1.75}Ge_{0.02}$ based CNT composites.[20, 38]

To further investigate the electronic effects Hall measurements were performed at room temperature on the reference sample and both samples containing 0.5 wt% CNT. Results are listed in Table I. Apparently, the addition of CNTs leads to a slight increase of the measured carrier concentration accompanied by a strong reduction of the

**Table I.** Room temperature Hall data of reference sample and both samples containing 0.5 wt% CNTs.

| Sample | Carrier concentration [$10^{20}$ cm$^{-3}$] | Carrier mobility [cm$^2$/Vs] |
|---|---|---|
| Reference sample | 2.6 | 30.1 |
| 0.5 wt% CNT, pestle-only prep. | 4.9 | 11.8 |
| 0.5 wt% CNT, ultrasonic prep. | 4.6 | 12.0 |

carrier mobility by 60%. While the increase of the carrier concentration would be expected to result in decreased Seebeck coefficients, this effect is overcompensated by the strong mobility reduction. Still, these values have to be handled with care as the samples with CNTs are obviously not homogeneous and thus Hall measurements are influenced by both components (skutterudite matrix, CNT agglomerates) and their geometric structure.

In agreement with the Seebeck coefficient's temperature dependence, the electrical conductivity is monotonically decreasing with increasing temperature in all samples. This is typical of highly doped semiconductors and a consequence of reduced mobility with increasing temperature. Independent of the preparation route the addition of CNTs leads to a reduction of the electrical conductivity. This effect is strongest for the samples with highest CNT content (Fig. 6). This reduction is strongest at low temperatures, thus effectively reducing the temperature dependence of the electrical conductivity. A similar behaviour was also observed by Itoh et al., when adding fullerene to a skutterudite matrix, and indicates scattering of carriers at grain boundaries/CNTs.[39] While the Seebeck coefficient is only affected by CNTs well dispersed and embedded in the matrix, the electrical conductivity is additionally sensitive to the large agglomerates: in these agglomerates the CNTs are rather loosely bound and not well connected to the skutterudite matrix. Thus, they behave similar to pores with regards to the electrical conductivity. The CNT concentration dependent component of the reduction of the electrical conductivity is thus probably a consequence of the large visible CNT agglomerates in the samples; similar to findings in composites of $CoSb_3$ and $C_{60}$ fullerene.[40] Additionally, a potentially constant

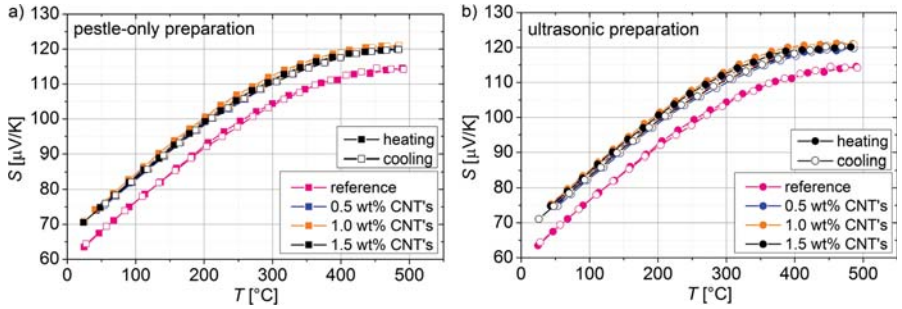


**Figure 5.** Temperature dependent Seebeck coefficient of samples prepared by pestle-only (a) and ultrasonic preparation (b). Seebeck coefficients rise with temperature; the addition of CNTs leads to a constant increase of the Seebeck coefficient independent of preparation route and CNT content.

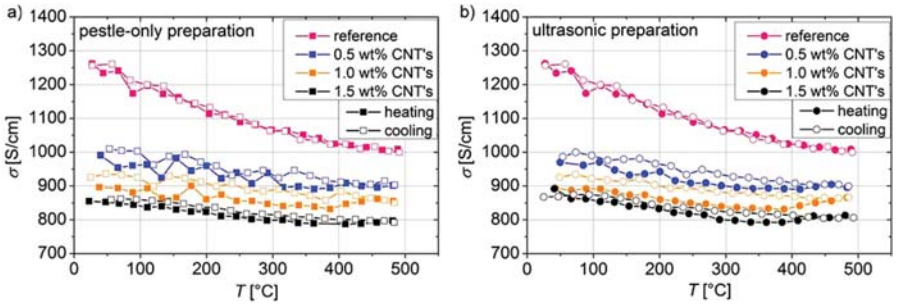


**Figure 6.** Temperature dependent electrical conductivity of samples prepared by pestle-only (a) and ultrasonic preparation (b). The conductivity decreases with temperature; the addition of CNTs leads to a concentration dependent reduction of the conductivity. No dependence on the preparation route is visible.

concentration of dispersed CNTs in the matrix in all samples causes an equal reduction of the electrical conductivity in all samples. These CNTs influence the microstructure and form additional barriers at grain boundaries, thus reducing the electrical conductivity via increased carrier scattering and a reduction of the carrier mobility.[20, 38] This approach of two separate effects would explain the big difference when going from 0 wt% to 0.5 wt% CNT, where both effects set in, compared to the small differences in the steps from 0.5 to 1.0 and 1.0 to 1.5, where the amount of dispersed CNTs in the matrix stays unchanged and thus a further reduction of the conductivity is caused by an increasing number of large agglomerates only.

SEM images taken on fresh fracture surfaces support this assumption. As can be seen in Figure 7, CNTs are not only found in large agglomerates (dark strips in Fig. 7(a)), but also as individual nano tubes or small networks of nano tubes at the grain boundaries within the skutterudite matrix (Fig. 7(b), lower left corner).

The conductivity of all samples increases slightly during the measurement cycle. Additional cycling during repeated measurements leads to no further changes in the electrical conductivity. This could be an indication of ongoing sintering in these samples at elevated temperatures during the first measurement. Still, no correlation between the amount of this conductivity change and the relative density of the samples is visible. Close investigation of the measured Seebeck coefficient values reveals, that values measured during the cooling phase of the measurements are slightly lower than during heating. Together with the observed change in electrical conductivity this indicates a slight increase of the charge carrier concentration during measurements, potentially as a result of changes in the phase composition or evaporation of antimony at higher temperatures.

As a result of the increased Seebeck coefficient and decreased electrical conductivity, the power factor $\sigma S^2$ is slightly reduced with increasing CNT content in the samples (Fig. 8). Again no significant difference between the two different preparation routes is visible.

Figure 9 displays the measured thermal conductivity of all samples. The thermal conductivity is nearly temperature independent at lower temperatures indicating a strong phonon scattering caused by the filler atoms. Above 350 °C the thermal conductivity increases in all samples, which is usually associated to bipolar contributions. In both preparation routes a strong initial reduction of the thermal conductivity is observed when increasing the CNT content from zero to 0.5 wt% and a further, yet weaker reduction when increasing the CNT content to higher values. The effect

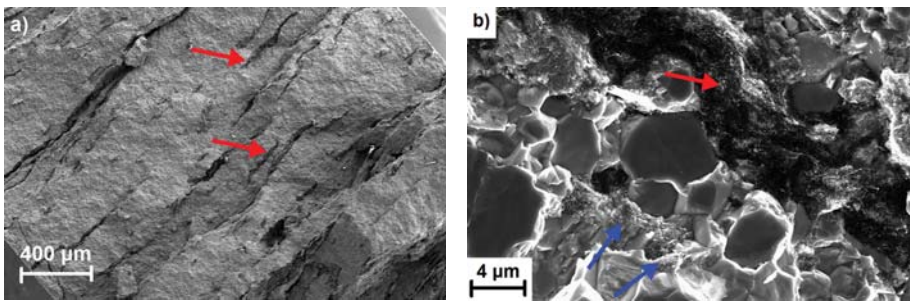


**Figure 7.** SEM images of fracture surfaces. Dark, elongated structures indicated by arrows in image (a) are agglomerates of CNTs forming layers perpendicular to the pressure during sintering in a 1.5 wt% CNT pestle-only sample. One such large agglomerate is visible as dark area spanning from the upper left to lower right corner in image (b), indicated by the red arrow. Furthermore small networks of CNTs at grain boundaries are indicated by blue arrows in the lower left corner of image (b).

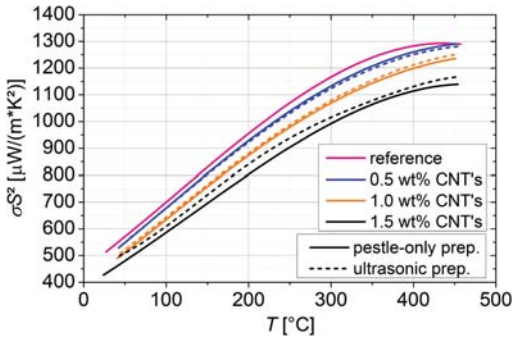


**Figure 8.** The temperature dependent power factor $\sigma S^2$ is slightly reduced upon the addition of carbon nanotubes as a result of the strong reduction of the electrical conductivity.

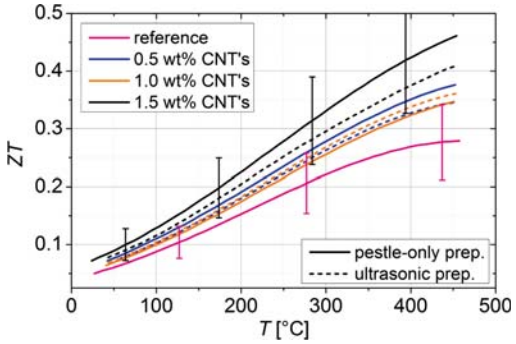


**Figure 10.** The thermoelectric figure of merit $ZT$ is increased upon addition of carbon nano tubes. Still, the influence of anisotropy on the measurement of the electrical and thermal conductivity has to be taken into account. Error bars result from the individual errors of the $S$, $\sigma$ and $\kappa$ measurement.

appears very similar in both preparation routes. An exception is the 1.5 wt% pestle-only sample. Its very low thermal conductivity is attributed to the significantly lower density compared to all other samples (see Fig. 3). In analogy to the explanations for the observed electrical conductivity, here again the reduction of the thermal conductivity might be a result of two individual contributions: first the phonon scattering by additional interfaces introduced by CNTs dispersed along the grain boundaries in the skutterudite matrix, and second pore-like structures on large scales due to CNT agglomerates.[20, 38, 41]

The reduction of the thermal conductivity is much stronger than of the electrical conductivity. This might be explained by anisotropy: the uniaxial pressure during sintering leads to rather flat, disc-like agglomerates of CNTs in a plane perpendicular to the mechanical pressure (see Fig. 7(a)). While the electrical conductivity measurement is done in parallel to these planes, thermal conductivity is measured cross plane. The barrier function of the large agglomerates ("pores") is naturally stronger for transport cross plane than in plane. Unfortunately, the measurement setups and sample geometries do not allow measurements in the respective other directions in order to compare electrical and thermal conductivity values measured in the same direction. Thus, the strong increase of the thermoelectric figure of merit $ZT$ with increasing CNT content shown in Figure 10 has to be taken with care and might be overestimated.

The influence of CNTs on the mechanical properties of the skutterudite composite material was investigated at room temperature by Vickers indentation, uniaxial compression and 4-point-bending tests. Results of these measurements are listed in Table II.

Hardness values are in good agreement with values for skutterudites without CNTs published elsewhere.[42] The addition of CNTs leads to a reduction of hardness, compressive and flexural strength. This reduction is strongest for the samples with highest CNT content, whereas no significant difference between both preparation methods can be observed except for the hardness values. This observed reduction of the mechanical strength is due to the formation of CNT agglomerates within the skutterudite matrix, effectively resulting in a porous material. Furthermore, the plane like agglomerates act as slip planes and planes in which cracks can easily propagate, thus leading to sample fracture already at low mechanical loads.[43] These results demonstrate the pivotal role of good dispersion and embedding of the CNTs within any host material to actually benefit from the tensile strength of the CNTs.[20, 44]

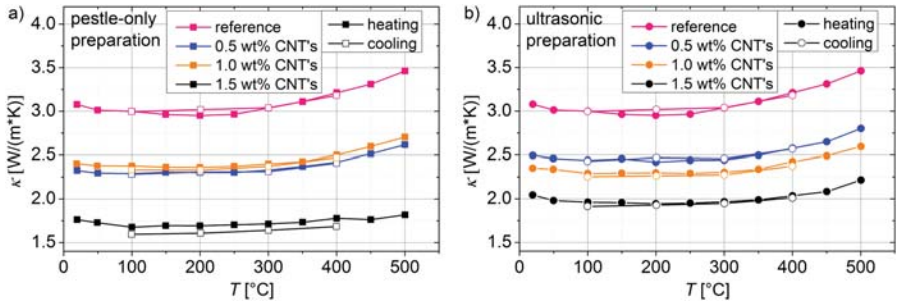


**Figure 9.** The addition of carbon nanotubes leads to a reduction of the thermal conductivity in both pestle-only (a) and ultrasonic preparation (b). The effect is stronger than in the electrical conductivity probably due to anisotropy caused by the layered structure of CNT agglomerates.

**Table II.** Room temperature mechanical properties of the pure $Ce_{0.14}La_{0.06}Co_2Fe_2Sb_{12}$ skutterudite sample ("reference") and CNT composites measured by Vickers indentation, uniaxial compression and 4-point-bending tests.

| Sample | CNT content wt% | Vickers hardness HV0.05 | Compressive strength MPa | Flexural strength MPa | Bending modulus GPa |
|---|---|---|---|---|---|
| Reference sample | 0 | 576 ± 52 | 630 ± 20 | 105 ± 10 | 44 ± 8 |
| Pestle-only prep. | 0.5 | 545 ± 60 | 370 ± 15 | 58 ± 8 | 35 ± 7 |
| | 1.0 | 563 ± 85 | 320 ± 15 | 54 ± 7 | 39 ± 8 |
| | 1.5 | 569 ± 70 | 255 ± 10 | 45 ± 5 | 33 ± 10 |
| Ultrasonic prep. | 0.5 | 513 ± 52 | 355 ± 15 | 65 ± 7 | 40 ± 6 |
| | 1.0 | 460 ± 72 | 380 ± 15 | 74 ± 8 | 43 ± 6 |
| | 1.5 | 437 ± 85 | 200 ± 10 | 60 ± 6 | 42 ± 6 |

## 4. CONCLUSIONS

Composites of skutterudites with carbon nano tubes have been prepared by mixing both components by grinding and by dispersion in an ultrasonic bath plus subsequent short term sintering. Although both preparation routes disperse a certain amount of CNTs at the grain boundaries within the skutterudite matrix, a considerable amount of the CNTs forms large agglomerates. While the dispersed CNTs lead to an increase of the Seebeck coefficient and increase carrier and phonon scattering, the agglomerated CNTs mainly act similar to pores and thus not only strongly reduce electrical and thermal conductivity, but also considerably weaken the composite material's mechanical strength. This proofs the pivotal role of the separation and a homogeneous distribution of carbon nano tubes in a skutterudite host material in order to achieve mechanical strengthening. Furthermore, the results indicate the potential improvement of the thermoelectric properties in these skutterudites. A possible route to reduce agglomeration and improve dispersion might be functionalization of the CNTs and more intense mixing of skutterudite and CNTs in a ball-mill. Furthermore, the results presented here indicate that low CNT concentrations of 0.5 wt% or less might be favorable.

**Acknowledgments:** The authors would like to thank the DFG for funding this research within the priority program SPP1386. Furthermore, we would like to thank our cooperation partners, the groups of Professor S. Schlecht (JLU Giessen, Germany) and Professor B. Paulus (FU Berlin, Germany) for providing the CNTs and helpful discussions.

## References and Notes

1. B. C. Sales, D. Mandrus, and R. K. Williams, *Science* 272, 1325 (**1996**).
2. R. Liu, J. Yang, X. Chen, X. Shi, L. Chen, and C. Uher, *Intermetallics* 19, 1747 (**2011**).
3. W. Y. Zhao, C. L. Dong, P. Wei, W. Guan, L. S. Liu, P. C. Zhai, X. F. Tang, and Q. J. Zhang, *J. Appl. Phys.* 102, 113708 (**2011**).
4. D. T. Crane and J. W. La Grandeur, *J. Electron. Mater.* 39, 2142 (**2010**).
5. A. F. Ioffe, Semiconductor Thermoelements and Thermoelectric cooling, Infosearch, London (**1957**).
6. G. Snyder, Thermoelectrics Handbook Macro to Nano, edited by D. M. Rowe, CRC Press, London (**2006**), pp. 81–102.
7. L. Liu, S. Sun, Q. Zhang, and P. Zhai, *J. Wuhan Univ. Technol. Mater. Sci. Ed.* 23, 415 (**2008**).
8. X. Yang, L. Liu, Q. Zhang, and P. Zhai, *J. Electron. Mater.* 40, 489 (**2011**).
9. S. Wan, X. Huang, P. Qui, S. Bai, and L. Chen, *Mater. Design* 67, 379 (**2015**).
10. V. Blank, S. Buga, V. Kulbachinskii, V. Kytin, V. Medvedev, and M. Y. Popov, *Phys. Rev. B* 86, 075426 (**2012**).
11. G. Tang, W. Yang, J. Wen, Z. Wu, C. Fan, and Z. Wang, *Ceram. Int.* 41, 961 (**2015**).
12. M. Kim, Y. Yeo, D. Park, and T. Oh, *Ceram. Int.* 38, 529 (**2012**).
13. F. Li, X. Huang, Z. Sun, J. Ding, J. Jiang, and W. Jiang, *J. Alloy Compd.* 509, 4769 (**2011**).
14. K. T. Kim and G. H. Ha, *J. Nanomater.* 2013, 8 (**2013**).
15. J. E. Morris, (ed.), Nanopackaging: Nanotechnologies and Electronics packaging, Edited by Springer, New York (**2008**), p. 345.
16. J. Hilding, E. A. Grulke, Z. G. Zhang, and F. Lockwood, *J. Disper. Sci. Technol.* 24, 1 (**2003**).
17. K. Balasubramanian and M. Burghard, *Chem. Unserer Zeit* 39, 16 (**2005**).
18. S. Bakshi, D. Lahiri, and A. Agarwal, *Int. Mater. Rev.* 55, 41 (**2010**).
19. B. Krause, M. Mende, P. Pötschke, and G. Petzold, *Carbon* 48, 2746 (**2010**).
20. F. Ren, H. Wang, P. A. Menchhofer, and J. O. Kiggans, *Appl. Phys. Lett.* 103, 221907 (**2013**).
21. D.-H. Park, M.-Y. Kim, and T.-S. Oh, *Curr. Appl. Phys.* 11, 41 (**2011**).
22. N. Gothard, G. Wilks, T. Tritt, and J. Spowart, *J. Electron. Mater.* 39, 1909 (**2010**).
23. Y. Zhang, X. Wang, W. Yeoh, R. Zheng, and C. Zhang, *Appl. Phys. Lett.* 101, 031909 (**2012**).
24. K. T. Kim, S. Y. Choi, E. H. Shin, K. S. Moon, H. Y. Koo, and G.-G. Lee, *Carbon* 52, 541 (**2013**).
25. X. Tang, L. Chen, T. Goto, and T. Hirai, *J. Mater. Res.* 16, 837 (**2001**).
26. J.-L. Mi, M. Christensen, E. Nishibori, and B. B. Iversen, *Phys. Rev. B* 84, 064114 (**2011**).
27. X. Meng, W. Cai, Z. Liu, J. Li, H. Geng, and J. Sui, *Acta Mater.* 98, 405 (**2015**).
28. J. Rodriguez-Carvajal, *Phys. B* 192, 55 (**1993**).
29. A. Schmitz, C. Stiewe, and E. Müller, *J. Electron. Mater.* 40, 543 (**2011**).
30. D. Platzek, G. Karpinski, C. Drasar, and E. Müller, *Mater. Sci. Forum* 492, 587 (**2005**).
31. J. de Boor, C. Stiewe, P. Ziolkowski, T. Dasgupta, G. Karpinski, E. Lenz, F. Edler, and E. Müller, *J. Electron. Mater.* 42, 1711 (**2013**).
32. J. de Boor and E. Müller, *Rev. Sci. Instrum.* 84, 065102 (**2013**).
33. A. Sesselmann, G. Skomedal, H. Middleton, and E. Müller, *J. Electron. Mater*. 45, 1397 (**2016**).
34. K. Mangersnes, O. M. Løvvik, and Ø. Prytz, *New J. Phys.* 10, 1 (**2008**).
35. C. Laurent, E. Flahaut, and A. Peigney, *Carbon* 48, 2994 (**2010**).
36. S. Katsuyama, Y. Shichijo, M. Ito, K. Majima, and H. Nagai, *J. Appl. Phys.* 84, 6708 (**1998**).
37. J. Peng, J. Yang, X. Song, Y. Chen, and T. Zhang, *J. Alloy Compd.* 426, 7 (**2006**).

**38.** D. Y. N. Truong, H. Kleinke, and F. Gascoin, *Dalton Trans.* 43, 15092 **(2014)**.
**39.** T. Itoh, K. Ishikawa, and A. Okada, *J. Mater. Res.* 22, 249 **(2007)**.
**40.** X. Shi, L. Chen, J. Yang, and G. P. Meisner, *Appl. Phys. Lett.* 84, 2301 **(2004)**.
**41.** X. Shi, L. D. Chen, S. Q. Bai, X. Y. Huang, X. Y. Zhao, Q. Yao, and C. Uher, *J. Appl. Phys.* 102, 103709 **(2007)**.
**42.** L. Zhang, G. Rogl, A. Grytsiv, S. Puchegger, J. Koppensteiner, F. Spieckermann, H. Kabelka, M. Reinecker, P. Rogl, W. Schranz, M. Zehetbauer, and M. A. Carpenter, *Mater. Sci. Eng. B* 170, 26 **(2010)**.
**43.** K. Shimoda, T. Hinoki, and A. Kohyama, *Compos. Sci. Technol.* 70, 387 **(2010)**.
**44.** R. Guzmán de Villoria and A. Miravete, *Acta Mater*. 55, 3025 **(2007)**.

Received: 14 March 2016. Accepted: 21 April 2016.